Benefit of coupling heparin to crosslinked collagen I/III scaffolds for human dermal fibroblast subpopulations' tissue growth

Anna Michopoulou, Eleni Koliakou, Zoi Terzopoulou, Patricia Rousselle, Artemis Palamidi, Doxakis Anestakis, Polyanthi Konstantinidou, Eva Roig-rosello, Euterpi Demiri, Dimitris Bikiaris

Benefit of coupling heparin to cross-linked collagen I/III scaffolds for human dermal fibroblast subpopulations' tissue growth.

Authors: Anna Michopoulou[1*], Eleni Koliakou[2], Zoi Terzopoulou[3], Patricia Rousselle[4], Artemis Palamidi[2], Doxakis Anestakis[5], Polyanthi Konstantinidou[5], Eva Roig-Rosello[4], Euterpi Demiri[6] and Dimitris Bikiaris[2*]

1. Biohellenika Biotechnology Company, Leoforos Georgikis Scholis 65, GR 555 35, Thessaloniki, Greece
2. Laboratory of Histology and Embryology, Medical School, Aristotle University of Thessaloniki, GR 541 24, Thessaloniki, Greece
3. Laboratory of Polymer Chemistry and Technology, Department of Chemistry, Aristotle University of Thessaloniki, Thessaloniki, Greece
4. Laboratoire de Biologie Tissulaire et Ingénierie Thérapeutique; UMR 5305; CNRS; Univ. Lyon 1; SFR BioSciences; 7 passage du Vercors, 69367, Lyon, France
5. Forensic Service of Thessaloniki, Department of Pathology, GR 57003, ThessalonikI, Greece
6. Department of Plastic Surgery, Medical School, Papageorgiou Hospital, Aristotle University of Thessaloniki, Thessaloniki, Greece

*Corresponding authors: dbic@chem.auth.gr (D.N.B.) and amichopoulou@biohellenika.gr (A.M.),

Note: E.K. and Z.T. contributed equally to the work

Keywords: Dermal equivalent, papillary and reticular dermis, histological morphology, collagen porous scaffold

ABSTRACT

There is currently lack of models representing the skin dermal heterogeneity for relevant research and skin engineering applications. This is the first study reporting production of dermal equivalents reproducing features of the papillary and reticular dermal compartments. Inspired from our current knowledge on the architecture and composition differences observed within the papillary and reticular dermis, we prepared and evaluated different collagen-based porous materials to serve as appropriate scaffolds for the three-dimensional expansion of freshly isolated papillary and/or reticular fibroblasts. The scaffolds, composed of either collagen I or mixed collagens I and III, were prepared by lyophilization. Pore size and hydrolytic stability were controlled by crosslinking with 1-ethyl-3-(3-dimethyl aminopropyl) carbodiimide (EDC) and N-hydroxysuccinimide (NHS) or EDC/NHS with covalently bound heparin. The evaluation of the resultant "papillary" and "reticular" dermal equivalents was based on the analysis of well-documented characteristic features of each dermal compartment, such as cell density and deposition of newly synthetized extracellular matrix components in histological sections. Our results demonstrate that crosslinking is important to support cell growth during the long procedure of dermal tissue formation independent on the fibroblast subpopulation. The presence of collagen III at the concentration used seemed to have some positive but non-specific effect only on the maintenance of the mechanical strength of the scaffolds during the long procedure of dermal formation. Our histological analyses demonstrated a significant and specific effect of heparin on generating dermal equivalents reproducing the respective higher papillary than reticular cell densities (~ 1.5 times more nuclei in all scaffolds containing heparin, $P \leq 0.04$) and supporting distinct extracellular matrix components deposition (3 to 5 times more carbohydrate material deposited by papillary fibroblasts in all scaffolds containing heparin, significancy P = 0.0001

to 0.05, while higher collagen production, compatible with reticular fibroblasts protein synthesis was observed only in the presence of heparin).

1. Introduction

The dermis is morphologically subdivided into the upper, papillary dermis adjacent to the basement membrane located below the epidermis and the reticular dermis, in the deeper layers overlying the adipose tissue [1], [2]. Each dermal compartment displays distinct architecture, extracellular matrix (ECM) composition [3] and functional roles in wound healing [4], skin aging [5][6], epidermal differentiation [5], scarring, fibrosis and cancer [7]. Fibroblasts are responsible for the production of the dense dermal ECM composed primarily of collagen I (80-85%) and collagen III (10-15%) [8], interconnected with other collagen subtypes, elastins and proteoglycans [9]. At least two different fibroblast subpopulations reside the dermal compartments, namely papillary fibroblasts (Pfbs) and reticular fibroblasts (Rfbs), each of them displaying specific properties [10][11][3][12].

The mechanisms behind the establishment of the dermal tissue heterogeneity are still unknown. Studying the properties as well as the interactions of the cells with the ECM in each dermal compartment will contribute to our understanding of the function of the dermis heterogeneity. However, there is currently a lack of models representing the dermal specific ECM patterning for relevant research. The papillary layer is a loose meshwork of thin, randomly oriented collagen fibers with a high fibroblast density [13]. Pfbs are described as lean, spindle-shaped cells, with high growth kinetics and low contractile properties [13][3][12]. Pfbs are primary source of dermal papilla synthesis during skin development and they are required for hair follicle formation in wound healing [14][15]. Increased expression of the Wnt signaling pathway components found in the papillary dermis is indicative of the reciprocal signaling with basal keratinocytes, which regulates both maintenance of the epidermal stem cell compartment and Pfbs cellular identity [16]. *In vivo* and *in vitro* studies showed that the papillary dermis has higher levels of collagen III and the dermatan surface proteoglycan, decorin and less chondroitin sulfate proteoglycan than the reticular dermis

[17][18]. Besides, only cultured primary Pfbs, unlike Rfbs, express the unconventional collagens found at the dermo-epidermal junction [19]. The central and largest reticular dermis, characterized by a low fibroblasts number, is composed of highly organized dense collagen fibers, elastin and woven reticular fibers providing this region with strength, extensibility and elasticity [20]. Rfbs have a more square and stretched appearance [3], [10], [12], they overexpress genes involved in cell motility, cytoskeletal organization and contraction and they are considered to mediate the early phase of wound repair [10][13]. Pfbs and Rfbs can be isolated based on unique morphological characteristics, gene expression profiles and cell surface markers [18]. Those include (1) the overexpression of podoplanin (PDPN) and netrin-1 for Pfbs, and matrix Gla protein and transglutaminase 2 for Rfbs, (2) higher proliferation capacity of Pfbs than Rfbs, (3) differential expression of matrisome-associated proteins such as collagen VII α1 chain, collagen XI α1 chain, and elastin. [3], [10], [12], (4) profiles of combination of surface markers such as CD26, CD39, CD36 (upper dermis: $lin^{-}CD90^{+}CD39^{+}CD26^{+}$, lower dermis: $lin^{-}CD90^{+}CD36^{+}$) [16], or CD90 and Fibroblast Activation Protein [11].

Collagen III is the second most abundant collagen in human dermis participating in collagen I fibrillogenesis and fiber diameter regulation [21], suggesting that its presence might be beneficial for the fate of both Pfbs and Rfbs. However, the lower collagen I/III ratio in the papillary dermis and the compromised collagen I/III ratio in pathological conditions, such as aging and hypertrophic scars suggest that its high expression around Pfbs might not be favorable [22]. ECM is no longer considered to be just an inert supportive material but is a source of spatial and temporal information to the cells via components such as the proteoglycans. A critical function of proteoglycans in the ECM is mediated by glycosaminoglycan (GAG) side chains, polysaccharide chains made up primarily of disaccharide units, which bind to growth factors, cytokines and chemokines with

considerable specificity. GAGs comprise chondroitin sulfate (CS), dermatan sulphate, keratan sulphate, heparin and heparan sulphate (HS) which are the most abundant. It is most likely that their precise distribution in the papillary and reticular dermal compartments may have an important impact on fibroblasts biology. GAGs are widely used in tissue engineering constructs to recapitulate the ECM. They are considered regulators of cell differentiation and maintenance of the phenotype of implanted cells [23][24], while through their negatively charged chains they can act as reservoirs for GFs and chemokines that finely control their release and therefore cell signaling [25]. Among GAGs, HS, heparin, and CS have a well-documented use as components of nanofibers for skin tissue engineering applications [24]. Heparin has the highest negative charge density of any biological macromolecule providing high affinity for growth factors (GFs), such as fibroblast growth factors and other factors important for wound healing [26][27]. For example, heparin was used as a small linker molecule in electrospun nanofiber scaffolds showing very promising results by improving crosslinking degree, enhancing the stability of scaffolds, forming complexes with different GFs and controlling their release [28][29].

The aim of this study was to produce dermal equivalents mimicking each dermal compartment. Inspired from our current knowledge on the architecture and composition differences observed within the papillary and reticular dermis, we prepared and evaluated different collagen- and heparin-based porous materials to serve as appropriate scaffolds for the three-dimensional (3D) expansion of freshly isolated Pfbs and/or Rfbs. To that end scaffolds were produced, analyzed and tested for their ability to support Pfbs or Rfbs.

2. Materials and Methods

2.1. Materials

Collagen (Bornstein and Traub Type I) from bovine achilles tendon was supplied by Sigma-Aldrich. Collagen (Bornstein and Traub Type III 90%, Type I <10%) from calf skin was supplied by YO Proteins AB. Heparin sodium was supplied by Fagron Hellas. N-(3-Dimethylaminopropyl)-N′-ethylcarbodiimide hydrochloride, N-Hydroxysuccinimide, acetic acid as well as all other chemicals used were of reagent grade and supplied by Sigma-Aldrich.

2.2. Preparation of porous collagen scaffolds

For the purposes of this study, we chose to produce natural nanofibrous scaffolds consisting of collagen I or a combination of collagen I and III to most closely mimic the fibrous component of the natural skin ECM [24]. By using cross-linking methods, we intended to adjust pore size and stiffness in the scaffolds with the aim to control cell density and resistance to cell contractility. Heparin was included to enhance the cross-linking and potentially influence cells growth and activity.

For the preparation of collagen I scaffolds, collagen I was dissolved in 0.2M acetic acid in a concentration of 1 wt%, in an ice bath to avoid denaturation. The heterogeneous solution was subjected to mechanical stirring with simultaneously short-term sonication using a sonicator probe in order to break down the aggregates. Afterwards, the viscous solution was homogenized with an Ultra-Turrax homogenizer for 5 min. Finally, centrifugation at 3500 rpm for 5 min took place to remove air bubbles and insoluble aggregates (calculated to be about 20 % of the initial mass). The resulting solution was placed in glass beakers, refrigerated and finally lyophilized with a ScanVac CoolSafe freeze dryer (Labogene,

Allerød, Denmark) at -60 °C and pressure 0.25 hPa to yield the collagen I scaffolds, denoted as Coll I.

The lyophilized Coll I scaffolds were crosslinked with EDC/NHS [30]. Briefly, crosslinking took place in a 4-morpholineethanesulfonic acid (MES) 0.05 M buffer solution with pH=5.4 in order to minimize EDC hydrolysis. Coll I scaffolds were initially washed with MES buffer and then immersed in an NHS/EDC solution in MES with NHS/EDC molar ratio=0.4. The reaction was left to proceed for 2.5 h and was stopped with the addition of a 0.1 M Na_2HPO_4 solution. The scaffolds were washed with deionized water, frozen at -20 °C and lyophilized to yield the scaffolds denoted as Coll I-Cross.

Immobilization of Heparin (Hep) was performed on the Coll I-Cross scaffolds [30]. For this, Coll I-Cross scaffolds were immersed in 0.05 M MES buffer (1 g in 188.3 mL buffer) for 30 min, followed by the addition of Hep in a final concentration of 1% w/v. To activate the carboxyl groups of NHS/EDC in a molar ratio 0.6 to Hep were added. The reaction took place for 2 h, followed by termination with 0.1 M Na_2HPO_4 solution and washing with 4 M NaCl and deionized water. The resulting scaffolds were lyophilized and are denoted as Coll-Cross-Hep.

The collagen I/III scaffolds were prepared by adding collagen III in a collagen I solution, prepared as described above, in a final concentration of 0.05 wt%. The scaffolds were lyophilized and are denoted as Coll I/III. Crosslinking and immobilization of Hep were performed in two steps, exactly as described for the Coll scaffold, and the scaffolds are denoted as Coll I/III-Hep.

2.3. Physicochemical characterization of scaffolds

The physicochemical and morphological properties of the scaffolds were evaluated with several methods including Fourier Transform Infrared Spectroscopy (FTIR), Scanning Electron Microscopy (SEM), swelling and enzymatic hydrolysis studies.

Fourier transform infrared spectroscopy (FTIR) spectra of the scaffolds were obtained using a Perkin-Elmer FTIR spectrometer, model Spectrum One.

The morphology of the scaffolds was examined with a JEOL JMS-840A SEM equipped with an energy-dispersive X-ray Oxford ISIS 300 microanalytical system (Oxford Instruments, Tubney Woods Abingdon, Oxfordshire, UK). All samples were coated with carbon black to avoid charging under the electron beam.

The swelling ability [31] of the scaffolds was evaluated by soaking pre-weighed 1x1 cm^2 pieces in Simulated Body Fluid (SBF), pH=7.4 and temperature 37 °C. Samples were removed at different time intervals, bloated with filter paper and weighed. The swelling ratio was calculated with the equation:

$$\text{Swelling ratio (\%)} = \frac{w_t - w_0}{w_0} x\ 100 \quad (1)$$

Where w_t is the weight of the scaffolds after soaking for different times and w_0 the initial weight of the scaffolds. The measurements were performed in triplicates.

Enzymatic hydrolysis rate of the scaffolds was studied by soaking them in SBF pH=7.4 that contained 2.5 mM $CaCl_2$ and collagenase type I (from Clostridium histolyticum) in a concentration 4000 ng/mL, at 37 °C. After predetermined time intervals, the scaffolds were removed from the medium, washed with deionized water and finally lyophilized. The enzymatic hydrolysis rate was calculated by the equation:

$$\text{Weight loss (\%)} = \frac{w_t - w_0}{w_0} x\ 100 \quad (2)$$

Where w_t is the final weight after enzymatic hydrolysis and w_0 the initial weight of the scaffolds. The measurements were performed in triplicates.

2.4. Isolation and cell culture

Biopsies from three female Caucasian donors aged at 39-46 years old subjected to aesthetic plastic surgeries (abdominal correction), withheld at the Papageourgiou General Hospital of Thessaloniki, were used for the isolation of keratinocytes and fibroblasts after their informed consent. Of all donors, both Pfbs and Rfbs were obtained from the upper and lower regions of interfollicular dermal tissue, respectively using a dermatome as described before [5]. All analyses were performed pairwise. Briefly, skin obtained from the surgery was cleaned thoroughly and stretched prior to be dermatomed at two different depths. First, a piece at a 300μm-depth was removed containing the epidermis and papillary dermis. Then, another deeper piece was removed including the reticular dermis. Fibroblasts and keratinocytes were isolated using the explant method as optimal for the isolation of adequate numbers of cells from small biopsies as described previously [32]. First, the epidermis was dissociated enzymatically from the dermis using treatment with 0.25% trypsin (BIOSERA, # LM-11720/100) for 2-4 h at 37 °C, 5% CO_2. For the isolation of the fibroblasts, the pieces of the dermis (papillary or reticular) were placed in culture in DMEM w/L-glutamine (BIOWEST, #L0104-500) supplemented with 10% fetal bovine serum (FBS) and penicillin-streptomycin (BIOWEST, # L0018-100) and maintained at 37 °C in a humidified atmosphere containing 5% CO_2. After migration of fibroblasts from the dermal explants, these cells were amplified in culture and stored in liquid nitrogen as frozen aliquots until use. The epidermis was placed with the basal membrane towards the bottom of a new culture plate, it was cut into very small pieces and maintained in DermaLife K basal medium (CELLSYSTEMS, # LL-004) supplemented with DermaLife K LifeFactors kit containing L-Glutamine, apo-transferrin, recombinant human (rh) transforming growth factor alpha (TGF-a), rh insulin,

hydrocortisone, epinephrine, bovine pituitary extract-BPE, gentamycin/amphotericin included in the kit (CELLSYSTEMS, # LS-1030) at 37 °C in a humidified atmosphere containing 5% CO_2 to let keratinocytes migrate from the explants. Keratinocytes were then frozen in liquid nitrogen until use for the present cell studies experiments.

2.5. Flow cytometry analysis

Fibroblasts cell lines (until passage 2) extracted from the papillary and reticular dermis were analyzed for the expression of transmembrane markers. Single cell suspensions were stained for FACS according to standard procedures using the FACS Calibur™ flow cytometer (BD Biosciences). Briefly, the cells were detached with trypsin and suspended in DMEM containing 10% FBS, then centrifuged at 1000 rpm for 5 min and suspended in PBS for staining and run. The primary antibodies used for FACS were: mouse monoclonal anti-human PDPN(E-1) conjugated to FITC (Santa Cruz Biotechnology, # sc-376695) (diluted 1:100), mouse monoclonal anti-human CD90 clone 5E10 conjugated to PE (BD Pharmingen, #555596) (diluted 1:100), mouse monoclonal anti-human CD-36 conjugated to FITC (Bio-Rad, # MCA722F), (diluted 1:100), 7-AAD (Viability Dye, Beckman Coulter, IMMUNOTECH, #IM360C).

MTT Proliferation assay

MTT assays were performed in 24-well plates. MTT was used for the comparison of proliferation rates between normal human Pfbs versus Rfbs *in vitro* and for the evaluation of cytocompatibility of the collagenous scaffolds (described in supplementary data). Early passage (p1) Pfbs and Rfbs from 3 different donors were seeded at 5,000 cells/well of a 96-well plate, in triplicates. The cells were left to grow until they reached 60% confluency and then, they were subjected to MTT proliferation assay. Briefly, the supernatant culture medium was removed and 100 ul of MTT (3-[4,5-Dimethylthiazole-2-yl]-2,5-

diphenyltetrazolium Bromide) at a concentration of 0.5mg/ml in DMEM was added to each well for a-4 h incubation at 37 °C, 5% CO2. Upon removal of the MTT, 1 mL/well of DMSO was introduced for 30 min at the same conditions. The reduction of MTT was counted at wavelengths 570/630 nm (Perkin Elmer).

2.6. Quantitative Real Time PCR analysis

Total RNA was isolated from monolayers using a Nucleospin RNA II kit (MACHEREY-NAGEL EURL, Hoerdt, France) according to manufacturer's instructions. 100 ng of total RNA extracted from fibroblasts of the papillary and reticular dermis (until passage 3) were subjected to the first strand cDNA synthesis and QPCR analysis using the KAPA SYBR FAST One-Step qRT-PCR KIT (KAPA BIOSYSTEMS). The primers used for the detection of gene expression PCNA and PDPN were designed on Primer-BLAST NIH software and are listed below. Reactions were performed using a Corbett 6000 real-time PCR cycler Rotorgene. The presence of a single dissociation peak was verified by melt curve analysis. Relative quantification was determined using the comparative (Ct) method with normalization to the housekeeping gene GAPDH.

PCNA - Forward: 5' -CTTACTGAGGGCGAGAAGCG- 3', Reverse: 5' –CTGAGACTTGCGTAAGGGAAGA-3',

PDPN - Forward: 5' –ACCAGTCACTCCACGGAGAA- 3', Reverse: 5' -GGCGTAACCCTTCAGCTCTT-3'

GAPDH - Forward: 5' –TGCACCACCAACTGCTTAGC- 3', Reverse: 5' -GGCATGGACTGTGGGTCATGAG- 3'

2.7. Preparation of dermal equivalents (DEs)

The scaffolds were disinfected in 70% ethanol overnight, washed 1 time in PBS and incubated in DMEM complete medium until use. For the preparation of the DEs, Pfbs or Rfbs (up to passage 4) were seeded at $5x10^4/cm^2$ in DMEM culture medium containing 1mM ascorbic acid 2-phosphate. After 21 days in culture, the DE were collected and fixed in neutral buffered formalin 10% for histological analysis.

2.8. Preparation of epidermalized skin equivalents (SEs)

For the preparation of epidermalized SE after 21 days of culture, keratinocytes were seeded on the DE at a density of $5x10^4/cm^2$ in a keratinocyte DermaLife K supplemented medium containing 1mM ascorbic acid 2-phosphate. After 7 days, the SE was elevated to the air-liquid interface and cultured for another 7 days in a differentiation medium consisting of 3:1 DMEM: Ham's F12 (BIOWEST) medium supplemented with 2% FBS, BPE (30µg/ml) and rh TGFα (10ng/ml).

2.9. Histological procedures on DEs

The DEs were left in 4% paraformaldehyde (PFA) solution for 24 h at 4 ^oC, then dehydrated in ascending alcohol concentrations and embedded in paraffin. Sections of 3µm were stained either with hematoxylin-eosin (H&E), using the Weigert-Van Gieson method and examined with an Axionlab light microscope. To evaluate collagen, elastin and glycoprotein-containing components within the dermal constructs, special histological stainings were performed including Masson's trichrome, orcein and Periodic Acid-schiff (PAS). Initially, the samples were subjected to deparaffinization independently on the subsequent staining protocol. Briefly, three consecutive xylene baths for 5 min followed by hydration of the sections with successive dilutions of alcohols (96%, 80%, and 70%) for 2 min each and finally washed under running water. For H&E staining, hematoxylin was added for 2:30 min, followed by differentiation with acetate alcohol (15 seconds), washed under running water and stained

with eosin for 2 min. To complete the procedure, the sections were dehydrated in ascending alcohols (70%, 96%, and 100%) for 2 min each and 3 consecutive xylene baths for 5 min. For Masson's trichrome staining, after deparaffinization and hydration of the sections the following staining procedure was performed: hematoxylin for 10 min, washing in running water, Ponceau Fuchsin drops for 5 min, washing with distilled water, staining with Phosphomolybdic acid for 10 min and staining with aniline blue for 5 min. After differentiation into acetic acid for 3 min, the sections were dehydrated in 96% alcohol for 2 min and 2 consecutive xylene baths for 2 min each. For elastin fibers staining, the slides were stained with orcein solution for 30 min, washing the slides in 70% alcohol for 10 min and washed with tap water. The sections were stained with hematoxylin for 1 minute, one dip in acid alcohol and finally the dehydration process and the 3 consecutive xylene baths described above. Finally, for PAS staining, the sections were oxidized for 10 min in periodic acid, washed in distilled water, immersed in the reagent Schiff's (a mixture of pararosaniline and sodium metabisulfite) for 20 min, followed by 3 changes in sulfur water for 6 min each, washed with running water, stained the sections with hematoxylin for 10 min and rinsed in tap water. For the covering and completion of the slides the process of dehydration and the 3 consecutive xylene baths was performed. Millipore's IHC Select® HRP / DAB detection kit (DAB150) and Cytokeratin 5 (Biolegend, # 01-46-9503) was used for immunohistochemical staining of the epidermalized samples. Deparaffinization was performed on PT module system, with pH retrieval high. Slides then incubated in PBS for 10 min, proteins were blocked for 5 min by the Blocking Reagent, antibodies were incubated for 30 min (Cytokeratin 5, 1: 200), then slides incubated for 10 min at secondary reagent (biotinylated goat anti-mouse IgG and goat anti-rabbit IgG in PBS, containing carrier protein) and finally 10 min incubation in Streptavidin HRP. Section staining was completed by adding DAB dye for 1 minute, washing with distilled water and then adding hematoxylin dye for 2 min. The

sections were immersed in 96% alcohol for 2 min, repeated 2 times and xylene baths alike and covered with cover strips.

2.10. Image analysis and processing

The H&E images were converted to 8-bit greyscale and manual counting of nuclei was performed using the ImageJ NIH software. Briefly, for the counting of cell nuclei/field, 3 different images per scaffold and fibroblast subpopulation were split in 10 squares of 1x1cm and the number of nuclei were counted per square. For each image, the number of nuclei per field was calculated as the mean of 10 squares. Each masson, orcein and PAS staining of the newly produced ECM was quantified using the ImageJ NIH software. Images were converted to 8-bit greyscale and areas containing cells surrounded by thin ECM meshwork were selected to overcome the strong non-specific background staining created by the scaffolds. After thresholding of the image, large colored surfaces were subtracted, eliminating remaining pieces of scaffold and cell bodies. The resulting small fibers were quantified. For each image, fibers quantification was related to the number of cells.

2.11. Statistical analysis

Data were presented as mean ± SD and the student's t-test (unpaired, two-tailed) was used for two groups comparisons. The exact sample size (n) and replicate measurements are specified in each graph legend. Differences were considered statistically significant at a value of $P<0.05$. The analysis was performed on the Graphpad Prism8 graphing and statistics software.

3. Results

3.1 Physicochemical and morphological characterization of the scaffolds

We produced the following scaffolds with different combinations of components mentioned above: (1) collagen I without cross-linking (Coll I) (2) crosslinked collagen I, using 1-ethyl-3-(3-dimethyl aminopropyl) carbodiimide (EDC) and N-hydroxysuccinimide (NHS) (Coll I-Cross), (3) EDC/NHS crosslinked collagen I with covalently combined heparin (Coll I-Cross-Hep), (4) collagen I+III (Coll I/III) (20:1 initial weight ratio) and (5) EDC/NHS crosslinked collagen I+III (Coll I/III-Cross-Hep) (20:1 initial weight ratio) with covalently combined heparin. A list of the prepared scaffolds, their abbreviations and compositions are presented in **Table 1.**

Table 1. Abbreviations and composition of the prepared collagen scaffolds.

Name	Collagen type	Cross-linking	Heparin immobilization
Coll I	I	No	-
Coll I-Cross	I	+	-
Coll I-Cross-Hep	I	+	+
Coll I/III	I, III	No	-
Coll I/III-Cross-Hep	I, III	+	+

The crosslinking reaction and subsequent heparin immobilization step are detailed in **Scheme 1**.

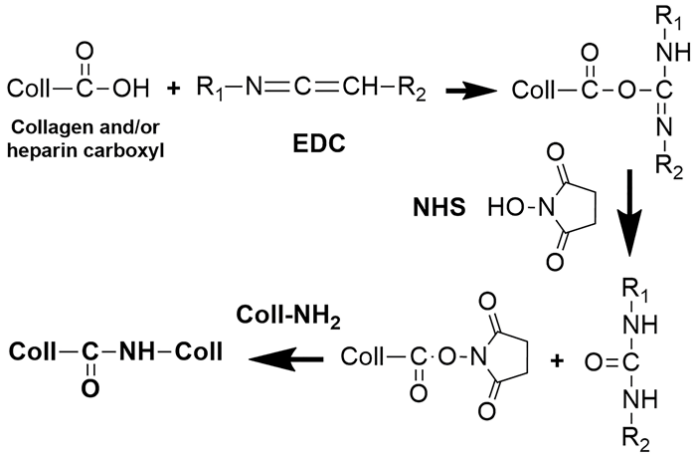

Scheme 1. Crosslinking reaction of collagen with NHS/EDC and immobilization of heparin.

Crosslinking of polymers with carboxylic end groups with NHS/EDC is widely used because of the non-cytotoxicity of the resulting products. The chemical structure of our scaffolds was examined by FTIR spectra as shown in **Figure 1**. Like all proteins, the peptide group is the one that gives the most characteristic bands in the spectrum of collagen. In the Coll I and the Coll I/III scaffolds, the amide A (N-H stretching vibrations) and amide B bands (asymmetrical C-H stretching) appear at ~3400 and 2930 cm^{-1}, respectively [33]. The amide I band that is associated mostly with C=O stretching appears at 1640 cm^{-1} and the amide II band of the N-H bending and the C-N stretching appears at 1550 cm^{-1} [34]. All these bands are also present in the spectra of the crosslinked scaffolds, with small shifts, and their presence after crosslinking witnesses the preservation of the secondary structure of collagen [35], [36], while the shift of the peak of amide I from 1640 cm^{-1} to 1635 cm^{-1} and 1638 cm^{-1} for Coll I-Cross and Coll I-Cross-Hep respectively suggests the weakening of the C=O bond of the peptide due to the formation of new bonds [37]. The band associated with amide II almost disappears in the Coll I-Cross-Hep scaffold, which is characteristic for crosslinked hydrogen scaffolds [35], [38].

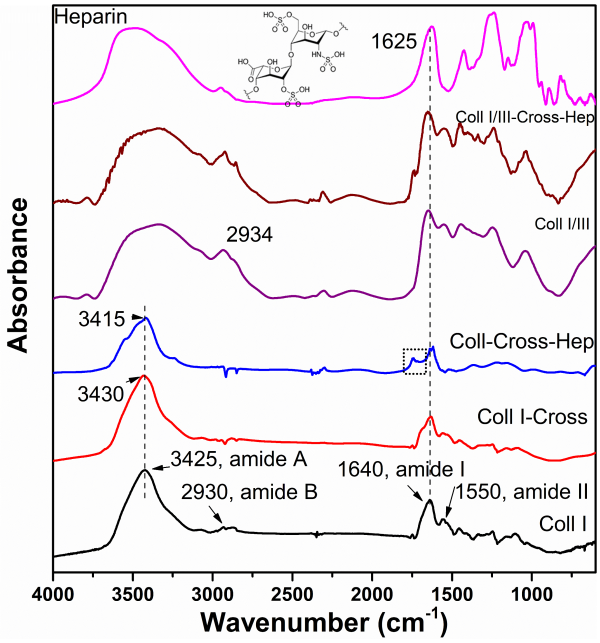

Figure 1. FTIR spectra of collagen scaffolds and heparin.

Heparin shows characteristic FTIR in the same regions as collagen [39]–[41], so no major differences can be observed between the spectra of Coll I and Coll I-Cross-Hep. However, a shoulder at 3550 cm^{-1} emerges and the peak at 1740 cm^{-1} increases greatly in intensity after the incorporation of heparin in collagen. This peak might be a result of the stretching vibration of carbonyls of side chains of amino acids or COOH terminal groups contained in the peptide chain of collagen [42], and its relative increase in relation to the amide I peak can be a result of the contribution of heparin's carboxyls to the crosslinking process, leaving more collagen's terminal carboxyl groups free. In summary, all the scaffolds produced in this study are found to have a preserved collagenic structure after their successful crosslinking.

The characteristics of the scaffolds were determined after SEM analysis, as presented in **Figure 2**. The micrographs of the Coll I scaffold (**Figure 2**a) illustrate the existence of an extensive, dense network of pores in 3D structures with heterogeneous pore size. The pores of Coll I/III are smaller, likely due to extensive shrinking during the preparation of the sample for analysis. Heterogeneity in the scaffold's microstructure, where pores of different sizes (i.e., larger localized density) are found in certain areas, can be attributed to the relatively high collagen concentration in the suspension used for scaffold preparation. In addition, some exposed collagen fibrils, which have not been reconstituted, are visible on the inner walls of the pores. The scaffolds possess pores smaller than 100 μm, enough to support the proliferation of reticular fibroblasts. Collagen matrices with pore diameters ranging from 50 to 100 μm are considered suitable for achieving biological activity [43].

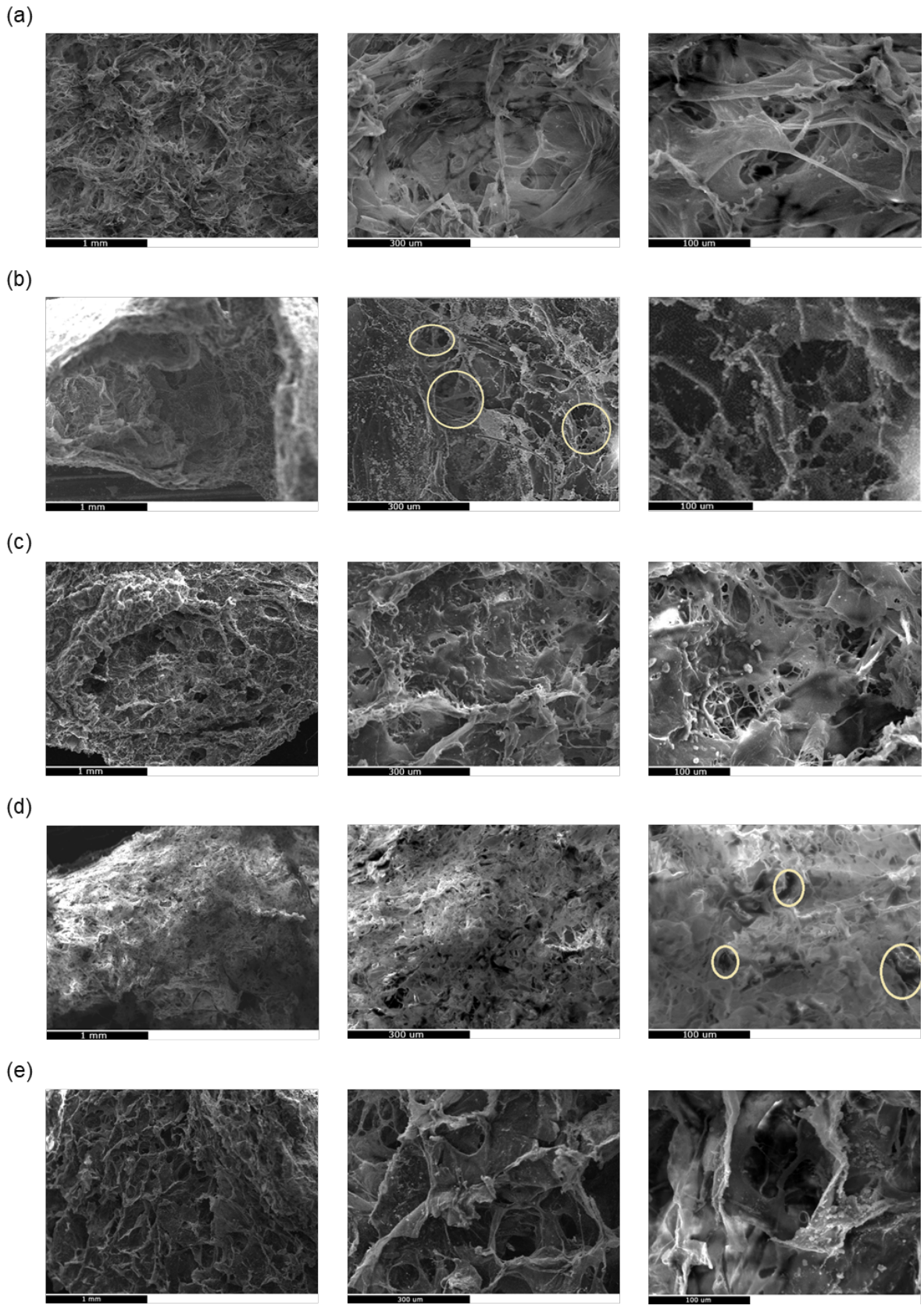

Figure 2. SEM micrographs of scaffolds (a) Coll I, (b) Coll I-Cross, (c) Coll I-Cross-Hep, (d) Coll I/III, (e) Coll I/III-Cross-Hep.

After crosslinking with EDC/NHS and EDC/NHS and heparin, extensive shrinking of the scaffolds occurred. It can be seen in the SEM micrographs that the extra steps of freezing and lyophilization resulted in aggregation of the collagen fibers, leading to the formation of some smaller pores while in other areas eventually larger pores are observed. The pore structure is more irregular but still present. Subsequently, SEM micrographs showed that crosslinking and heparin immobilization had a significant effect on the porosity of the scaffolds.

In the context of the evaluation of morphological characteristics and structural stability of the scaffolds, the swelling ratio after immersion in SBF was determined. The ability of the scaffold to retain water is an important parameter, as increased swelling rates are associated with increased cell adhesion and proliferation [44]. The test continued until the weight values stabilized after 2 h, when equilibrium was reached. The results are presented in **Figure 3**a. The porous scaffolds prepared are capable of absorbing large amounts of SBF, with swelling ratios up to ~ 1000 %. A rapid increase in the swelling rate was observed in all scaffolds during the first few min of immersion, and afterwards the weight values stabilized for longer immersion times. Coll I/III scaffolds presented the highest swelling abilities. Crosslinking with EDC/NHS resulted in a significant reduction in their swelling capacity. Coll I swelled up to ~ 623 %, whereas this value decreased to ~ 390 % for Coll I-Cross and ~ 490 % for Coll I-Cross-Hep. Coll I/III swelled up to ~ 1100%, and after crosslinking its swelling decreased to ~ 1000 %. The collagen's swelling properties can be attributed to changes in the hydrophilicity caused by the decrease in the number of free amino and carboxyl side groups available for the formation of hydrogen bonds with water [45]. Next, the formation of additional amide bonds results in an extensive crosslinking network that gives a more compact structure with reduced fluid retention capacity. The crosslinking and subsequent lyophilization caused shrinking and reduction of the porosity as previously

mentioned, therefore as smaller amounts of water can be retained in the structure of the scaffolds, the overall swelling ability reduced. As for the slightly higher swelling ratio value of Coll I-Cross-Hep compared to Coll I-Cross, it can be attributed to the hydrophilicity of the heparin's sulfate groups and its subsequent retention of excess water [46], [47].

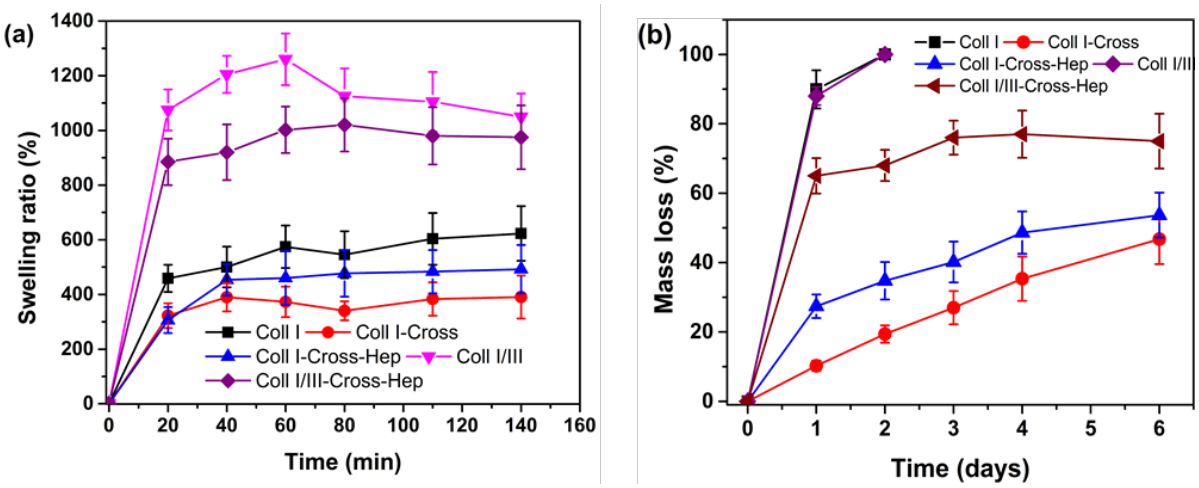

Figure 3. Swelling ratio % in SBF and (b) mass loss % of the collagen scaffolds during enzymatic hydrolysis (n=3).

In **Figure 3**b, the mass loss % of the scaffolds during enzymatic hydrolysis at 37 °C is depicted. The non-crosslinked scaffolds fully degraded after 2 days of soaking in the hydrolysis media, while the crosslinked scaffolds presented a much slower mass loss rate, in agreement with previous studies [47]–[49]. After 2 days, Coll I-Cross and Coll I-Cross-Hep lost 19.4±2.5 % and 34.7±5.4 % of their mass. Coll I/III-Cross-Hep lost 75±7.9 % of its initial mass. The extent of collagen's degradation depends on the density of crosslinks and the accessibility of enzymes to cleavage sites. The crosslinks block the access of the enzymes to specific cleavage sites stereochemically, as they are "hidden" by the introduction of new bonds, thereby reducing the rate of degradation. Typically, the affinity of the enzyme for the substrate is reduced due to the presence of new amide bonds, which affect the electrostatic interactions that develop and therefore the enzyme activity. Subsequently, fragments from the

collagen matrices are retained by the crosslinking molecules and therefore additional cleavage is necessary for the release of peptide fragments [50]. The crosslinking process of our Coll I scaffolds enhanced their bio-stability. It should be noted here that Coll I-Cross-Hep is slightly more prone to enzymatic degradation than Coll I-Cross, most likely due to its increased hydrophilicity. Both the increased swelling and faster enzymatic hydrolysis of the scaffolds that contain both types of collagen can be attributed to the structural differences between collagen I and III. The lack of helicity in the trypsin-susceptible region and the variation in its helicity in general could be the underlying reasons for the observed differences [51].

3.2 Distinct morphology, proliferation profile and expression of surface markers of fibroblast subpopulations extracted from the papillary and reticular dermis.

In this study, dermatome was used to dissect the papillary and reticular dermis from human skin biopsies. The fibroblasts were maintained in culture until passage 3 (**Figure 4**). The isolated fibroblasts subpopulations were characterized after their expansion *in vitro*, based on their morphological characteristics according to previously validated criteria [4]. Representative images are shown in **Figure 4**a, Pfbs presented a spindle-shaped morphology while Rfbs were flattened cells. Pfbs responded immediately to post-seeding *in vitro* cell culture expansion reaching confluency after three days. Instead, Rfbs only started to proliferate three days after seeding. The increased proliferative capacity after 3 days in culture, as shown by the MTT analysis, was confirmed at the gene transcription level by QPCR analysis of the expression of the proliferating marker PCNA (Proliferating Cell Nuclear Antigen) (**Erreur ! Source du renvoi introuvable.**b). We further assessed the expression of PDPN in Pfbs by flow cytometry as well as gene transcription level by QPCR (**Figure 4**c). Another test was also performed to analyze the presence of CD90+/CD36+ cells with pre-adipogenic capacity as suggested recently [11] that are normally found at the deeper

reticular dermis adjacent to the underlying adipose tissue (**Figure 4**d). These results confirmed the efficient isolation and expansion of two enriched subpopulations of fibroblasts to be used for the purposes of this study despite the fact that we do not have pure populations of Pfbs and Rfbs but rather two groups of cells into which one subtype predominates.

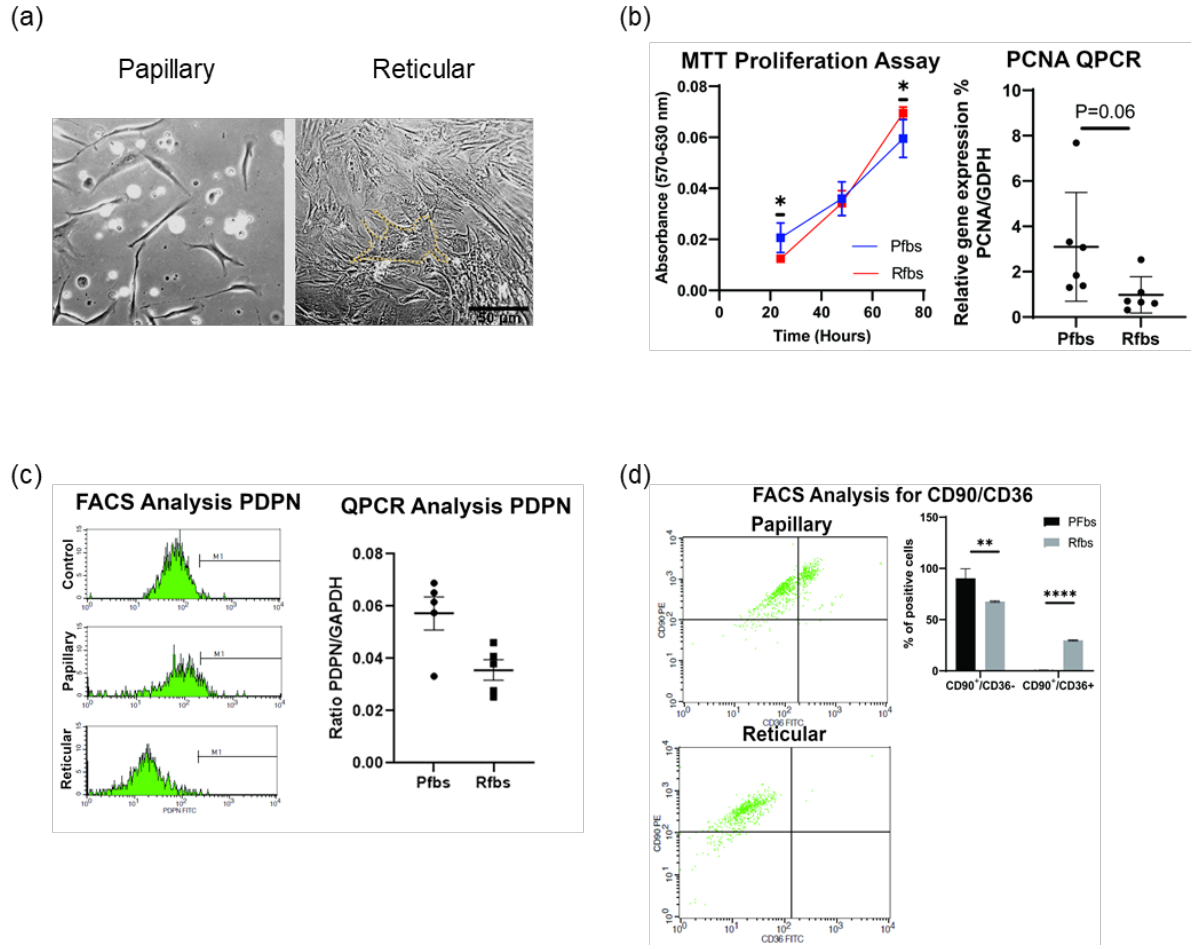

Figure 4. Confirmation of fibroblasts subpopulations. (a) Bright field images showing different morphologies of fibroblasts extracted from the papillary and reticular dermis. (b) Histograms showing the cell proliferation rates of fibroblasts from the papillary and reticular dermis analyzed by MTT and QPCR analysis of PCNA in matched pairs of passage 3 fibroblasts from three donors in duplicates. For PCNA analysis RNA was collected from cells after 72 hours (3 days) of culture. (c) QPCR and flow cytometry analysis of the papillary marker PDPN (podoplanin) in matched pairs of third passage fibroblasts from three donors in duplicates. Control corresponds to fibroblasts extracted from full dermis (d) Flow cytometry analysis of CD90+/CD36+ fibroblasts. Error bars represent mean±SD. (Asterisks indicate P-values; <0.05*, <0.01**, <0.0001****, n_donors=3).

3.4 Evaluation of dermal equivalents obtained from Pfbs and Rfbs 3D cultures.

Pfbs or Rfbs were seeded within the scaffolds and left to grow in cell culture. After 4 weeks, DEs were fixed and embedded in paraffin for basic histological examinations to visualise and quantify general cell distribution and ECM deposition (**Figure 5 and 6**). Masson and PAS stainings already revealed discernible thin, differentially stained tissue intertwined in the large scaffold meshes in all conditions, desmonstrating that cell culture conditions were viable and allowed ECM deposition (Figure 5 a, b). Coll I scaffolds without crosslinking could not support dermal formation due to the loss of stability during culture and therefore they could not be further evaluated but they only served as a control of biocompatibility (Supplementary data).

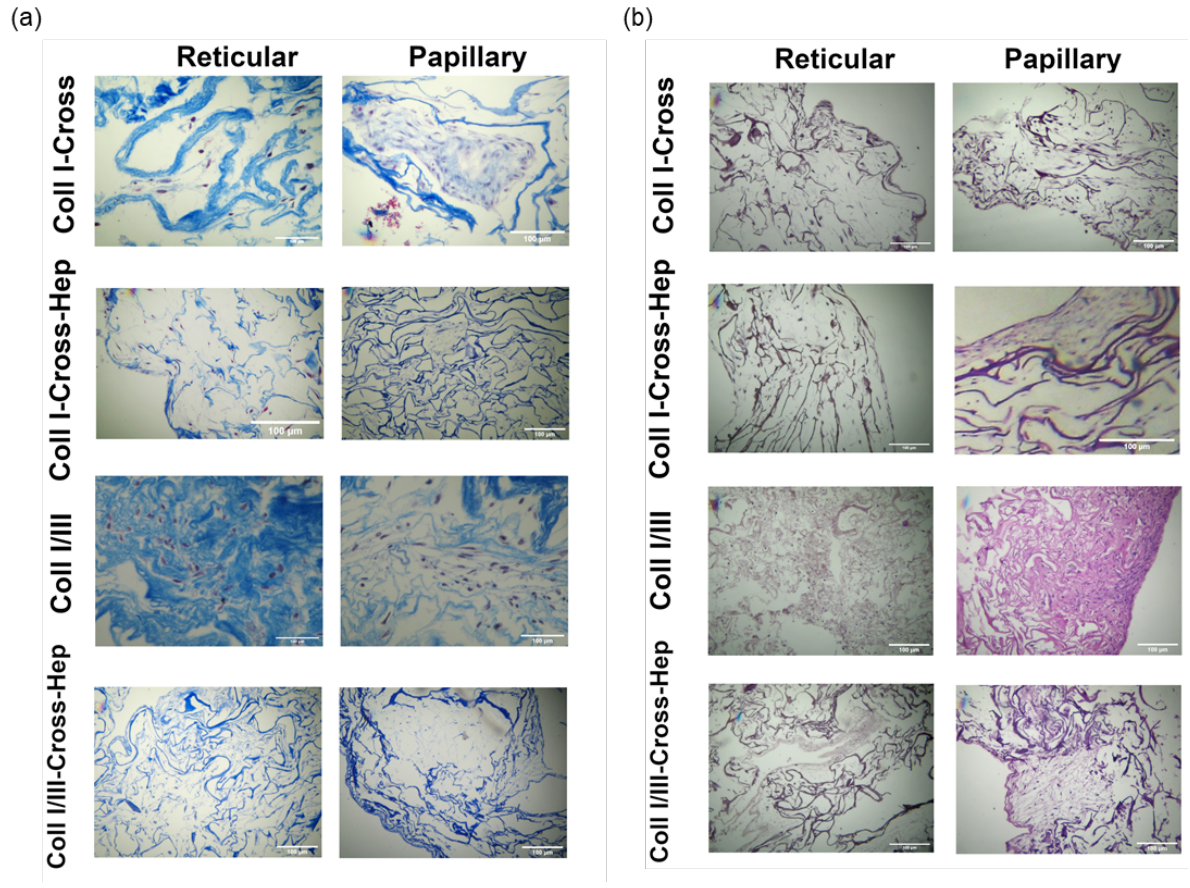

Figure 5. Histological staining of Coll I-Cross, Coll I-Cross-Hep, Coll I/III and Coll I/III-Cross-Hep based DEs. Scale bar: 50μm (a) Masson staining was used for the visualization of new collagen material synthetized and deposited by Pfbs and/or Rfbs on each scaffold. (b) PAS staining was used for the visualization of new material containing carbohydrates.

Haematoxylin and eosin staining was then performed to visualize the overall structure of both Pfbs- and Rfbs-DEs and evaluate cell colonisation (**Figure 6**). As shown in **Figure 6**a-b, the numbers of Pfbs found in the scaffolds were higher than those of Rfbs, which is in line with their different rates of proliferation. In the crosslinked scaffolds containing heparin, these differences were statistically significant independent on the presence of collagen III, suggesting that heparin is favourable to the preservation of each of the 2 fibroblasts populations' proliferative phenotype.

(a)

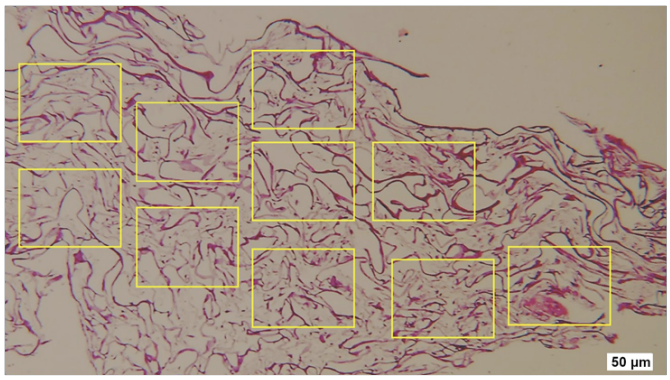

(b)

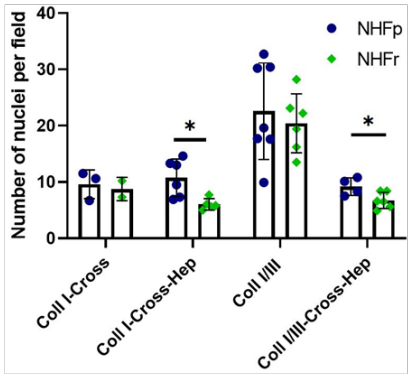

(c)

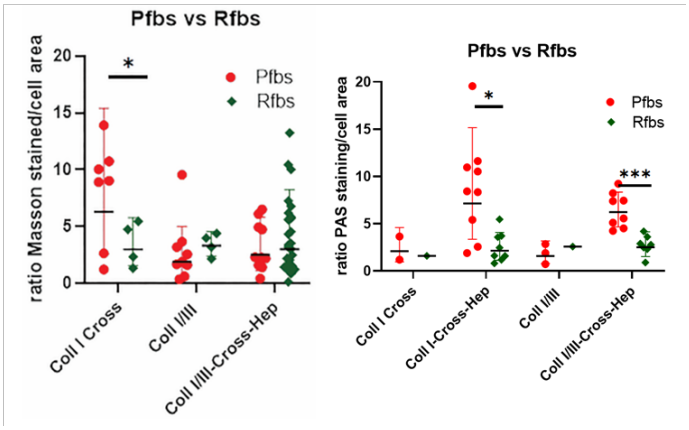

Figure 6. Evaluation of different collagen-based porous scaffold to support Rfbs- and/or Pfbs- derived dermis. (a) Presentation of the method of quantification of cell nuclei in the DEs after H&E staining of histological sections. (b) Statistical analysis of nuclei counting. For nuclei counting each image was divided in 10 equal squares and the mean number of nuclei per image is presented on the graph. At least 2 independent experiments were performed per scaffold condition. (c) Evaluation of newly synthetized ECM on the DEs after quantification of the applied staining on histological sections. Quantification is expressed as ratio of Masson stained area/cell area and ratio of PAS stained area/cell area. Each counting is presented on the graph. (Asterisks indicate P-values; <0.05*, <0.001***).

The higher number of nuclei found in the Coll I/III scaffold for both Pfbs and Rfbs is likely an artefact derived from the contraction imposed by the cells on these scaffolds that resulted in an important shrinkage at the end of the procedure. Therefore, the high amount of cell nuclei is not indicative of the higher proliferating ratio but it is likely a result of the decrease of the surface area as a function of the number of nuclei. This can be due to the lack of collagen crosslink causing, as we shown in **Figure 3**b, a lack of stability and stiffness followed by a rapid degradation. In contrast, crosslinked scaffolds maintained their architecture all along the growth procedure.

In order to evaluate the deposition of ECM components by Pfbs and Rfbs into the different scaffolds, specialized histological staining techniques were applied. Collagen and glycoprotein were stained by Masson's trichrome and PAS respectively. Quantification of each individual staining was expressed as mean stained area / cell for each histological section (**Figure 6**c). Data were collected from at least 3 independent experiments per fibroblast subpopulation, unless otherwise mentioned. Rfbs produced more, although not statistically significant, collagen after culture within Coll I/III and Coll I/III-Cross-Hep scaffolds. In the Coll I-Cross scaffold, the amount of collagen detected around Pfbs was significantly higher than that detected in the Rfbs environment. Quantification of PAS staining, used to visualize carbohydrates, glycogen, glycoproteins and basement membranes, demonstrated that Pfbs cultured in the tested cross-linked scaffolds deposited more

carbohydrate material/cell than Rfbs. This difference was significant when the Coll I/III-Cross-Hep and Coll I-Cross-Hep were used suggesting that heparin had an advantageous impact on glycoprotein synthesis. The very low amount of protein found within the Coll I/III scaffold may be linked to the high proliferative rate of the cells in this non-crosslinked scaffold.

As a first attempt on evaluating the Coll I/III-Cross-Hep scaffold to support epithelialization, we added human keratinocytes to assay the formation of an epidermis on "papillary" dermal equivalent produced by using Pfbs (**Figure 7**). Our preliminary keratin 5 staining suggests that a viable epithelium was formed indicating that production of skin equivalents including a Pfbs-colonized dermis will be possible in the future.

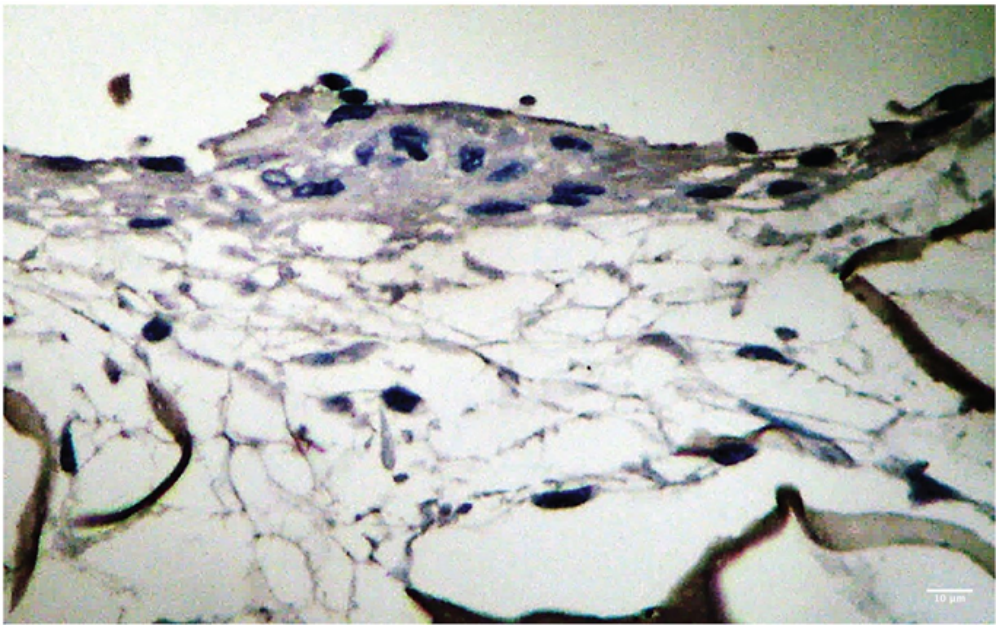

Figure 7. Evaluation of epidermal growth over Coll I/III-Cross-Hep based-DE.

4. Discussion

The use of 3D cell cultures gains progressively ground over 2D cultures in both pharmacological assays and basic research because a 3D microenvironment provides more

reliable outcomes [52]. Dermo-epidermal or epidermal-engineered skin grafts have long been used for the treatment of burns and chronic wounds as clinical skin substitutes but also as models in applied and basic research [53][54]. Skin tissue engineering requires a 3D biomaterial serving as a scaffold for fibroblasts to expand and form dermal tissue and subsequent seeding of keratinocytes to form an epidermis. Engineering of skin equivalents is challenging technically and demands detailed optimization of every parameter of this step-by-step procedure resulting in a multilayered structure.

Biomaterials offer more than a mechanical support for the attachment and growth of cells; they also provide biochemical signals that modulate their behavior. Therefore, one major issue for an efficient biomaterial is to mimic as closely as possible the structure and composition of the native ECM of the tissue [54] consisting of collagens, elastin, GAGs and hyaluronic acid [55]. The ECM also works as a deposit for GFs controlling their bioavailability. The ECM architecture influences material stiffness and thus, regulates cellular behavior through rearrangements of the cytoskeleton and cell signaling, while regulates/facilitates cell infiltration [55]. Considering the complexity and the incomplete understanding of ECM composition and structure, it is understandable that creating a scaffold that fully mimics the biochemistry and architecture of native tissue is rather unlikely [54]. Acellular dermal matrices (ADMs) derived from decellularized skin and other tissue sources have shown promising clinical results in tissue repair and their preparation requires several processings to reduce immunogenicity and prevent infection [22]. At the same time, the techniques used should preserve the structural and biochemical properties of the ECM which is not always the case since every decellularized method disrupts to some degree the ECM [54], [55]. Besides, standard criteria for tissue decellularization have not been officially described [54]. Human de-epidermized dermis (DED) presents the advantage of retaining the native structure of the dermal ECM by containing the papillary and reticular layers, a

technical challenge in 3D scaffolds [56]. However, DEDs are donors-derived which limit their availability and display low reproducibility related to individual donor differences.

Synthetic scaffolds are less representative of the native dermal structure, but they are reproducible; they can be easily modified and are available for *in vitro* model settings and development. Stuart and Panitch found that adding collagen III in gels of collagen I resulted in decreased fibril diameter and stiffness, and increased rate of collagen fibrillogenesis [57]. Chondrogite™, a commercial collagen I/III sponge is being used in chondrogenesis [58], while reports have been published on the successful vocal fold tissue regeneration [59], nerve reconstruction [60] and corneal regeneration with collagen I/III scaffolds [61]. Fibroblast grown on Chondrogite™ present with a spinocellular shape, and form a thick layer of large cells that is strongly adhered to the matrix [62]. Heparin is a sulphate polysaccharide with binding affinity for several GFs including platelet-derived growth factor (PDGF), FGF and others. GFs are important regulators of cellular behaviour such as proliferation, but they are often unstable in aqueous solutions. Therefore, it is difficult to maintain their high local concentration in culture conditions. To solve this problem, several groups assayed crosslinking collagen in sponge scaffolds using heparin with very encouraging results [58][59][60].

In this study, we produced and evaluated collagen-based porous scaffolds with the aim to mimic papillary and reticular dermis features. The scaffolds were designed based on the hypothesis that by controlling the stiffness and pore size within the scaffolds by using crosslinking methods we might be able to control the rate of cell growth and density of each fibroblast subpopulation with the aim to mimic the physiological conditions. Pfbs are more spindle-like and they reside within a more loosen ECM as compared to Rfbs that are quite bigger cells and reside in a dense network of collagen. Then, by adding Collagen III was thought to likely favor Pfbs since some studies, as mentioned earlier, have shown that

collagen III predominates within the papillary dermis as compared to collagen I which is the predominant type in the reticular dermis. Therefore, different collagen composition and crosslinking methods were used to regulate scaffolds' architecture, stiffness and pore size.

The scaffolds were produced and evaluated progressively. Firstly, Coll I, ColI I-Cross and Coll I-Cross-Hep were produced and examined for cytocompatibility. Coll I alone without any crosslinking although presented good cell viability it could not stand long cell culture as it was extremely contracted by the cells. Therefore, it was not chosen for the future experiments but served as a control of cytocompatibility for the first experiments. Then, Collagen III was introduced in the scaffolds and Col I/III without crosslinking was produced. The cells were successfully cultured in those scaffolds and although there was a lot of contraction it was still possible to further process them and assess them for new ECM deposition. Coll I/III-Cross-Hep was the scaffold produced next. The evaluation of the first three scaffolds for both fibroblasts subpopulations concluded that the presence of heparin is beneficial for the growth of both fibroblast types, while crosslinking is also necessary because of the contraction problems. Therefore, and in order to limit the cost, Coll I/III-Cross-Hep was produced next and Coll I/III-Cross was excluded.

To sum up, all the selected scaffolds were tested for their ability to support Pfbs and Rfbs culture and formation of dermal tissue. We could show that all the scaffolds assayed in this study were successful in supporting 3D fibroblast growth from both dermal compartments and we confirmed the importance of material crosslinking for scaffold stability and tissue growth independent on the fibroblasts subtype. However, the fibroblasts subtypes populations we obtained were not of total purity due to the extraction method we used, each of the papillary and reticular were sufficiently enriched to display the expected and previously validated phenotype characteristics. By adding collagen III at a ratio of 1:20 to scaffolds without crosslinking we could improve stability without obtaining more specific

results after further evaluation of the dermal equivalents. This preliminary result suggests a positive effect of the presence of collagen III on the scaffolds stability. However, a more specific biological effect on Pfbs and/or Rfbs cannot be excluded since we only used one and very low concentration of collagen III in our scaffolds, the potential impact of a specific collagen I/III ratio on cells' behavior was not examined here and last but not least we did not use pure populations of Pfbs and Rfbs. In contrary, the use of heparin as a linker in the scaffolds resulted in reproducible dermal equivalents with distinct cell growth and ECM deposition characteristics after seeding of Pfbs or Rfbs independent on scaffolds' collagen composition. We revealed for the first time a potential impact of heparin on the preservation of Pfbs and Rfbs respective proliferative phenotype in crosslinked collagen scaffolds. Our preliminary examination of new deposited ECM revealed that Pfbs produced significantly more glycoproteins than Rfbs, while Rfbs produced more even non-significant collagen than Pfbs, which is compatible with protein synthesis by Rfbs in human skin [6][19]. A hypothesis might be that the presence of heparin functions as a reservoir for the GFs present in the culture medium and/or produced by the fibroblasts regulating their balanced disposal to the cells thus, driving their behaviour. Altogether, results obtained with the Coll I/III-Cross-Hep scaffolds appeared more reproducible for both Pfbs and Rfbs. To further evaluate our Coll I/III-Cross-Hep based 'papillary' dermal equivalents we assayed the formation of an epithelium after seeding human keratinocytes. Our preliminary results showed the formation of a viable yet not properly differentiated epidermis. Although encouraging these experiments require improvement and standardization.

Our study is the first to report a beneficial impact of heparin as a linker in crosslinked collagen I/III scaffolds on the formation of papillary and reticular dermal equivalents.

5. Conclusions

To our knowledge, this is the first study that attempted to create and evaluate different collagen porous scaffolds for the specific papillary or reticular dermal formation upon seeding of human skin Pfbs or Rfbs. This study demonstrates that fibroblasts from different dermal compartments may respond differently when seeded onto scaffolds of the same composition and mechanical properties and vice versa. Our findings are also confirmatory and/or complementary of other recent matrisome analysis research studies which demonstrate that Pfbs and Rfbs present a different ECM synthesis profile due to different factors including genetics, microenvironment, aging, etc [19][6]. Our principal conclusions on the different scaffolds used for this study are summarized as follows: (1) Crosslinking is necessary for the maintenance of scaffolds stability during the long tissue culture procedure independent on the cell subtype, (2) collagen III at the concentration used for these experiments seemed to have only a non-specific positive effect on the maintenance of scaffolds architecture. (3) The presence of heparin had a significant, reproducible and specific effect on the generation of papillary and reticular dermal equivalents presenting higher Pfbs than Rfbs cell densities at the same culture conditions and distinct ECM components deposition. This study highlights the benefit of heparin presence as a linker in collagen porous scaffolds independent on the presence of collagen III and the cell subtype. This effect may be attributed to the property of this GAG to act as a deposit and regulator of GFs release in the scaffolds. The importance of collagen III for the production of papillary and reticular dermal equivalents deserves to be further investigated in the future by producing and evaluating scaffolds with different collagen I/III ratios and by using pure Pfbs and Rfbs populations.

Acknowledgments

We acknowledge the contribution of SFR Biosciences (UAR3444/CNRS, US8/Inserm, ENS de Lyon, UCBL) facilities, more precisely Jacques Brocard from PLATIM, for his help in quantifying the histological stainings. We also acknowledge the Department of Plastic Surgery of General Hospital Papageorgiou in Thessaloniki for providing us with skin biopsies.

Funding

This research has been co-financed by European Union and Greek national funds through the Operational Program Competitiveness, Entrepreneurship, and Innovation, under the call RESEARCH–CREATE–INNOVATE (project T1EΔK-03798) and a Rhône-Auvergne Pack Ambition Recherche 2020 to PR.

REFERENCES

[1] F. M. Watt and H. Fujiwara, “Cell-extracellular matrix interactions in normal and diseased skin.,” *Cold Spring Harb. Perspect. Biol.*, 2011, doi: 10.1101/cshperspect.a005124.

[2] R. R. Driskell, C. A. B. Jahoda, C. M. Chuong, F. M. Watt, and V. Horsley, “Defining dermal adipose tissue,” *Experimental Dermatology*. 2014, doi: 10.1111/exd.12450.

[3] M. Ghetti *et al.*, “Subpopulations of dermal skin fibroblasts secrete distinct extracellular matrix: implications for using skin substitutes in the clinic,” *Br. J. Dermatol.*, 2018, doi: 10.1111/bjd.16255.

[4] D. G. Janson, G. Saintigny, A. Van Adrichem, C. Mahé, and A. El Ghalbzouri, “Different gene expression patterns in human papillary and reticular fibroblasts,” *J. Invest. Dermatol.*, vol. 132, no. 11, pp. 2565–2572, 2012, doi: 10.1038/jid.2012.192.

[5] S. Mine, N. O. Fortunel, H. Pageon, and D. Asselineau, “Aging alters functionally human dermal papillary fibroblasts but not reticular fibroblasts: A new view of skin morphogenesis and aging,” *PLoS One*, 2008, doi: 10.1371/journal.pone.0004066.

[6] V. Haydont, V. Neiveyans, N. O. Fortunel, and D. Asselineau, “Transcriptome profiling of human papillary and reticular fibroblasts from adult interfollicular dermis pinpoints the ‘tissue skeleton’ gene network as a component of skin chrono-ageing,” *Mech. Ageing Dev.*, vol. 179, no. December 2018, pp. 60–77, 2019, doi: 10.1016/j.mad.2019.01.003.

[7] M. D. Lynch and F. M. Watt, “Fibroblast heterogeneity: implications for human disease,” *J. Clin. Invest.*, vol. 128, no. 1, pp. 26–35, 2018, doi: 10.1172/JCI93555.

[8] W. Cheng, R. Yan-Hua, N. Fang-Gang, and Z. Guo-An, “The content and ratio of type

I and III collagen in skin differ with age and injury," *African J. Biotechnol.*, vol. 10, no. 13, pp. 2524–2529, 2011, doi: 10.5897/AJB10.1999.

[9] M. D. Lynch and F. M. Watt, "Fibroblast heterogeneity: implications for human disease," *Journal of Clinical Investigation*. 2018, doi: 10.1172/JCI93555.

[10] D. G. Janson, G. Saintigny, A. Van Adrichem, C. Mahé, and A. El Ghalbzouri, "Different gene expression patterns in human papillary and reticular fibroblasts," *J. Invest. Dermatol.*, 2012, doi: 10.1038/jid.2012.192.

[11] A. Korosec *et al.*, "Lineage Identity and Location within the Dermis Determine the Function of Papillary and Reticular Fibroblasts in Human Skin," *J. Invest. Dermatol.*, 2019, doi: 10.1016/j.jid.2018.07.033.

[12] P. Nauroy *et al.*, "Human Dermal Fibroblast Subpopulations Display Distinct Gene Signatures Related to Cell Behaviors and Matrisome," *J. Invest. Dermatol.*, 2017, doi: 10.1016/j.jid.2017.03.028.

[13] G. Sriram, P. L. Bigliardi, and M. Bigliardi-Qi, "Fibroblast heterogeneity and its implications for engineering organotypic skin models in vitro," *European Journal of Cell Biology*. 2015, doi: 10.1016/j.ejcb.2015.08.001.

[14] Y. Rinkevich *et al.*, "Identification and isolation of a dermal lineage with intrinsic fibrogenic potential," *Science (80-.).*, 2015, doi: 10.1126/science.aaa2151.

[15] R. R. Driskell *et al.*, "Distinct fibroblast lineages determine dermal architecture in skin development and repair," *Nature*, 2013, doi: 10.1038/nature12783.

[16] C. Philippeos *et al.*, "Spatial and Single-Cell Transcriptional Profiling Identifies Functionally Distinct Human Dermal Fibroblast Subpopulations," *J. Invest. Dermatol.*, vol. 138, no. 4, pp. 811–825, 2018, doi: 10.1016/j.jid.2018.01.016.

[17] J. M. Sorrell and A. I. Caplan, “Fibroblast heterogeneity: More than skin deep,” *Journal of Cell Science*. 2004, doi: 10.1242/jcs.01005.

[18] D. Jiang and Y. Rinkevich, “Defining skin fibroblastic cell types beyond CD90,” *Front. Cell Dev. Biol.*, vol. 6, no. OCT, pp. 1–3, 2018, doi: 10.3389/fcell.2018.00133.

[19] A. Mauroux *et al.*, “Papillary and reticular fibroblasts generate distinct microenvironments that differentially impact angiogenesis,” *bioRxiv*, 2020, doi: 10.1101/2020.11.29.402594.

[20] E. Rognoni and F. M. Watt, “Skin Cell Heterogeneity in Development, Wound Healing, and Cancer,” *Trends in Cell Biology*. 2018, doi: 10.1016/j.tcb.2018.05.002.

[21] H. P. Bächinger, K. Mizuno, J. A. Vranka, and S. P. Boudko, “5.16 - Collagen Formation and Structure,” H.-W. (Ben) Liu and L. B. T.-C. N. P. I. I. Mander, Eds. Oxford: Elsevier, 2010, pp. 469–530.

[22] M. Dussoyer, A. Michopoulou, and P. Rousselle, “Decellularized scaffolds for skin repair and regeneration,” *Appl. Sci.*, vol. 10, no. Application of Extracellular Matrix in Regenerative Medicine, p. 3435, 2020, doi: https://doi.org/10.3390/app10103435.

[23] H. Sodhi and A. Panitch, “Glycosaminoglycans in tissue engineering: A review,” *Biomolecules*, vol. 11, no. 1, pp. 1–22, 2021, doi: 10.3390/biom11010029.

[24] L. Bacakova *et al.*, “Nanofibrous Scaffolds as Promising Cell Carriers for Tissue Engineering,” *Nanofiber Res. - Reach. New Height.*, 2016, doi: 10.5772/63707.

[25] A. Weyers and R. J. Linhardt, “Neoproteoglycans in tissue engineering,” *FEBS J.*, vol. 280, no. 10, pp. 2511–2522, 2013, doi: 10.1111/febs.12187.

[26] F. Aleahmad *et al.*, “Fabrication and characterization of heparin/collagen sponge for in vitro differentiation of Wharton’s jelly-derived mesenchymal stem cells into

hepatocytes," *Hepat. Mon.*, vol. 17, no. 2, 2017, doi: 10.5812/hepatmon.40599.

[27] E. Bellu, S. Medici, D. Coradduzza, S. Cruciani, E. Amler, and M. Maioli, "Nanomaterials in skin regeneration and rejuvenation," *Int. J. Mol. Sci.*, vol. 22, no. 13, 2021, doi: 10.3390/ijms22137095.

[28] Y. R. Chen *et al.*, "Low-Molecular-Weight Heparin-Functionalized Chitosan-Chondroitin Sulfate Hydrogels for Controlled Release of TGF-β3 and in vitro Neocartilage Formation," *Front. Chem.*, vol. 7, no. November, pp. 1–16, 2019, doi: 10.3389/fchem.2019.00745.

[29] A. Vijayan, N. C. K., and G. S. Vinod Kumar, "ECM-mimicking nanofibrous scaffold enriched with dual growth factor carrying nanoparticles for diabetic wound healing," *Nanoscale Adv.*, vol. 3, no. 11, pp. 3085–3092, 2021, doi: 10.1039/d0na00926a.

[30] M. J. B. Wissink *et al.*, "Immobilization of heparin to EDC/NHS-crosslinked collagen. Characterization and in vitro evaluation," *Biomaterials*, vol. 22, no. 2, pp. 151–163, 2001, doi: 10.1016/S0142-9612(00)00164-2.

[31] T. K. Ã and H. Takadama, "How useful is SBF in predicting in vivo bone bioactivity ? $," vol. 27, pp. 2907–2915, 2006, doi: 10.1016/j.biomaterials.2006.01.017.

[32] Z. Terzopoulou, A. Michopoulou, A. Palamidi, E. Koliakou, and D. Bikiaris, "Preparation and evaluation of collagen-based patches as curcumin carriers," *Polymers (Basel).*, 2020, doi: 10.3390/polym12102393.

[33] R. J. Jakobsen, L. L. Brown, T. B. Hutson, D. J. Fink, and A. Veis, "Intermolecular interactions in collagen self-assembly as revealed by Fourier transform infrared spectroscopy," *Science (80-.).*, vol. 220, no. 4603, pp. 1288–1290, 1983.

[34] T. Riaz *et al.*, "FTIR analysis of natural and synthetic collagen," *Appl. Spectrosc. Rev.*,

vol. 53, no. 9, pp. 703–746, 2018.

[35] A. Sionkowska, J. Skopinska-Wisniewska, M. Gawron, J. Kozlowska, and A. Planecka, “Chemical and thermal cross-linking of collagen and elastin hydrolysates,” *Int. J. Biol. Macromol.*, vol. 47, no. 4, pp. 570–577, 2010.

[36] Š. Rýglová, M. Braun, and T. Suchý, “Collagen and its modifications—crucial aspects with concern to its processing and analysis,” *Macromol. Mater. Eng.*, vol. 302, no. 6, p. 1600460, 2017.

[37] R. Usha, K. J. Sreeram, and A. Rajaram, “Stabilization of collagen with EDC/NHS in the presence of l-lysine: A comprehensive study,” *Colloids Surfaces B Biointerfaces*, vol. 90, pp. 83–90, 2012.

[38] T. Suchý *et al.*, “The effects of different cross-linking conditions on collagen-based nanocomposite scaffolds—an in vitro evaluation using mesenchymal stem cells,” *Biomed. Mater.*, vol. 10, no. 6, p. 65008, 2015.

[39] A. Devlin, L. Mauri, M. Guerrini, E. A. Yates, and M. A. Skidmore, “The use of ATR-FTIR spectroscopy to characterise crude heparin samples by composition and structural features,” *bioRxiv*, p. 744532, 2019.

[40] D. Gonzalez, J. Ragusa, P. C. Angeletti, and G. Larsen, “Preparation and characterization of functionalized heparin-loaded poly-Ɛ-caprolactone fibrous mats to prevent infection with human papillomaviruses,” *PLoS One*, vol. 13, no. 7, p. e0199925, 2018.

[41] H. Z. Zhang, R. S. Li, N. Wang, L. Qi, C. Z. Huang, and J. Wang, “Heparin sodium-selective ‘on–off’and lysine-selective ‘off–on’fluorescence switching of cadmium telluride quantum dots and their analytical applications,” *Anal. Methods*, vol. 8, no. 2,

pp. 453–459, 2016.

[42] S. Y. Venyaminov and N. N. Kalnin, “Quantitative IR spectrophotometry of peptide compounds in water (H2O) solutions. I. Spectral parameters of amino acid residue absorption bands,” *Biopolymers*, vol. 30, no. 13□14, pp. 1243–1257, Jan. 1990, doi: 10.1002/bip.360301309.

[43] F. J. O’Brien, B. A. Harley, I. V Yannas, and L. J. Gibson, “The effect of pore size on cell adhesion in collagen-GAG scaffolds,” *Biomaterials*, vol. 26, no. 4, pp. 433–441, 2005.

[44] L. Ma *et al.*, “Collagen/chitosan porous scaffolds with improved biostability for skin tissue engineering,” *Biomaterials*, vol. 24, no. 26, pp. 4833–4841, 2003.

[45] Y. Xu *et al.*, “Physiochemical and biological properties of modified collagen sponge from porcine skin,” *J. Wuhan Univ. Technol. Sci. Ed.*, vol. 24, no. 4, pp. 619–626, 2009.

[46] B. Kaczmarek, A. Sionkowska, and J. Skopinska-Wisniewska, “Influence of glycosaminoglycans on the properties of thin films based on chitosan/collagen blends,” *J. Mech. Behav. Biomed. Mater.*, vol. 80, pp. 189–193, 2018, doi: https://doi.org/10.1016/j.jmbbm.2018.02.006.

[47] M. Ansari, S. S. Kordestani, S. Nazralizadeh, and H. Eslami, “Biodegradable cell-seeded collagen based polymer scaffolds for wound healing and skin reconstruction,” *J. Macromol. Sci. Part B*, vol. 57, no. 2, pp. 100–109, 2018.

[48] C. Kilic Bektas, I. Kimiz, A. Sendemir, V. Hasirci, and N. Hasirci, “A bilayer scaffold prepared from collagen and carboxymethyl cellulose for skin tissue engineering applications,” *J. Biomater. Sci. Polym. Ed.*, vol. 29, no. 14, pp. 1764–1784, 2018.

[49] X. Lim, M. Potter, Z. Cui, and J. F. Dye, “Manufacture and characterisation of EmDerm—novel hierarchically structured bio-active scaffolds for tissue regeneration,” *J. Mater. Sci. Mater. Med.*, vol. 29, no. 6, p. 79, 2018.

[50] N. A. Danilov *et al.*, “Stabilization of scleral collagen by glycerol aldehyde cross-linking,” *Biochim. Biophys. Acta (BBA)-General Subj.*, vol. 1780, no. 5, pp. 764–772, 2008.

[51] H. G. Welgus, R. E. Burgeson, J. A. M. Wootton, R. R. Minor, C. Fliszar, and J. J. Jeffrey, “Degradation of monomeric and fibrillar type III collagens by human skin collagenase. Kinetic constants using different animal substrates,” *J. Biol. Chem.*, vol. 260, no. 2, pp. 1052–1059, 1985, doi: 10.1016/s0021-9258(20)71207-x.

[52] A. Idrees *et al.*, “Validation of in vitro assays in threedimensional human dermal constructs,” *Int. J. Artif. Organs*, 2018, doi: 10.1177/0391398818775519.

[53] P. Rousselle, F. Braye, and G. Dayan, “Re-epithelialization of adult skin wounds: Cellular mechanisms and therapeutic strategies,” *Adv. Drug Deliv. Rev.*, vol. 146, pp. 344–365, 2019, doi: 10.1016/j.addr.2018.06.019.

[54] G. S. Hussey, J. L. Dziki, and S. F. Badylak, “Extracellular matrix-based materials for regenerative medicine,” *Nature Reviews Materials*. 2018, doi: 10.1038/s41578-018-0023-x.

[55] A. Dasgupta *et al.*, “A novel reticular dermal graft leverages architectural and biological properties to support wound repair,” *Plast. Reconstr. Surg. - Glob. Open*, 2016, doi: 10.1097/GOX.0000000000001065.

[56] L. Costello *et al.*, “Engineering a multilayered skin equivalent: The importance of endogenous extracellular matrix maturation to provide robustness and reproducibility,”

in *Methods in Molecular Biology*, 2019.

[57] K. Stuart and A. Panitch, "Characterization of gels composed of blends of collagen I, collagen III, and chondroitin sulfate," *Biomacromolecules*, vol. 10, no. 1, pp. 25–31, 2008.

[58] N. Shaikh, M. K. T. Seah, and W. S. Khan, "Systematic review on the use of autologous matrix-induced chondrogenesis for the repair of articular cartilage defects in patients," *World J. Orthop.*, vol. 8, no. 7, p. 588, 2017.

[59] T. Walimbe, S. Calve, A. Panitch, and M. P. Sivasankar, "Incorporation of types I and III collagen in tunable hyaluronan hydrogels for vocal fold tissue engineering," *Acta Biomater.*, vol. 87, pp. 97–107, 2019, doi: 10.1016/j.actbio.2019.01.058.

[60] G. Keilhoff, F. Stang, G. Wolf, and H. Fansa, "Bio-compatibility of type I/III collagen matrix for peripheral nerve reconstruction," *Biomaterials*, vol. 24, no. 16, pp. 2779–2787, 2003, doi: 10.1016/S0142-9612(03)00084-X.

[61] P. Fagerholm *et al.*, "Stable corneal regeneration four years after implantation of a cell-free recombinant human collagen scaffold," *Biomaterials*, vol. 35, no. 8, pp. 2420–2427, 2014, doi: 10.1016/j.biomaterials.2013.11.079.

[62] M. Fuss, E.-M. Ehlers, M. Russlies, J. Rohwedel, and P. Behrens, "Characteristics of human chondrocytes, osteoblasts and fibroblasts seeded onto a type I/III collagen sponge under different culture conditions: a light, scanning and transmission electron microscopy study," *Ann. Anatomy-Anatomischer Anzeiger*, vol. 182, no. 4, pp. 303–310, 2000.